

## Non-Abelian Holonomy in Degenerate Non-Hermitian Systems

Zhong-Lei Shan,<sup>†</sup> Yi-Ke Sun,<sup>†</sup> Ran Tao, Qi-Dai Chen<sup>ORCID</sup>, Zhen-Nan Tian, and Xu-Lin Zhang<sup>ORCID</sup>\*

*State Key Laboratory of Integrated Optoelectronics, College of Electronic Science and Engineering,  
Jilin University, Changchun 130012, China*

 (Received 26 February 2024; revised 1 June 2024; accepted 10 July 2024; published 2 August 2024)

Non-Abelian holonomy, a noncommutative process that measures the parallel transport of non-Abelian gauge fields, has so far been realized in degenerate Hermitian systems with degenerate eigenstates or nondegenerate non-Hermitian systems with exceptional points. Here, we introduce non-Abelian holonomy into degenerate non-Hermitian systems possessing degenerate exceptional points and degenerate energy topologies. The interplay between energy degeneracy and energy topology around exceptional points leads to a non-Abelian holonomy with multiple energy levels and multiple degenerate levels simultaneously, going beyond that in degenerate Hermitian systems with a single energy level, or in nondegenerate non-Hermitian systems with a single degenerate level. We exploit an on-chip photonic platform to experimentally demonstrate the holonomy induced non-Abelian phenomenon, including the switching of eigenstates associated with different degenerate exceptional points and sequence-dependent holonomic outcomes. Our work shifts the paradigm of non-Abelian holonomy and adds new degrees of freedom for non-Abelian applications.

DOI: [10.1103/PhysRevLett.133.053802](https://doi.org/10.1103/PhysRevLett.133.053802)

In physics, holonomy refers to a phenomenon that arises when a state of a system is adiabatically transported around a closed loop in Hilbert space but fails to preserve its initial status due to the associated nontrivial gauge fields [1–4]. A well-known example of holonomy is Berry phase [5], which is a gauge invariant scalar quantity associated with an Abelian gauge field. Gauge fields can also be non-Abelian in nature, meaning that the induced consequences are noncommutative. The resulted matrix-valued non-Abelian holonomy has played a pivotal role in various areas of physics [6–9], and has been realized in various physical systems including neutral atoms [10,11], acoustic systems [12,13], superconductors [14], and photonic systems [15–20]. These systems are Hermitian systems and the holonomy is realized via the construction of a degenerate eigenspace that supports multiple degenerate eigenstates occupying the same energy level. Non-Abelian Berry-Wilczek-Zee phase matrix [2] appears when these degenerate states are simultaneously evolving in Hilbert space. Holonomy can also be realized in non-Hermitian systems when there exist exceptional points (EPs) [21–23]. The topology of the energy surface around EPs allows the switching of eigenstates at different energy levels by encircling the EPs. This process has been demonstrated in various nondegenerate non-Hermitian systems based on stroboscopic experiments [24–28] and dynamical experiments [29–35]. The non-Hermitian holonomy can exhibit

non-Abelian features when the system possesses two or more EPs [36].

These two non-Abelian schemes imply that the non-Abelian holonomy is associated with multiple degenerate levels but only one energy level in degenerate Hermitian systems [see Fig. 1(a) for a schematic], while that in nondegenerate non-Hermitian systems has multiple energy levels but only one degenerate level [see Fig. 1(b)]. This straightforwardly indicates that the paradigm and physical consequence of non-Abelian holonomy can be greatly enriched by realizing a holonomic process with multiple energy levels and multiple degenerate levels simultaneously. Apparently, such process would require a degenerate eigenspace with multiple degenerate EPs (DEPs) and associated degenerate energy topologies, where the holonomy induced eigenstate transformation can occur simultaneously between different energy levels and degenerate levels [see Fig. 1(c)]. However, research in this direction has been elusive, either in theory or experiment.

Here, we propose the design principle and experimental realization of the non-Abelian holonomy in degenerate non-Hermitian systems. We construct a six-state non-Hermitian system consisting of degenerate three-state subsystems, in which two DEPs are respectively supported. By enforcing path-dependent hopping coefficients, on-site energies and on-site non-Hermitian losses, two eigenstates associated with one DEP can be adiabatically pumped to those associated with the other DEP, leading to a non-Abelian holonomy with two energy levels and two degenerate levels. All the available holonomic operations in the proposed system are found to form a non-Abelian

<sup>†</sup>These authors contributed equally to this work.

\*Contact author: xulin\_zhang@jlu.edu.cn

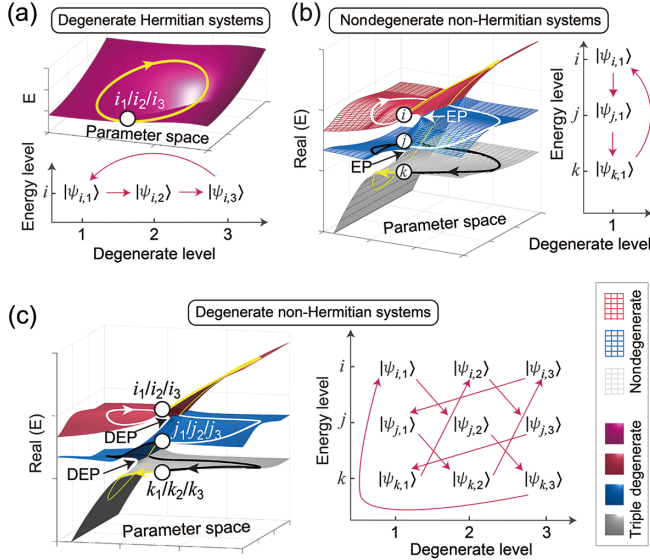


FIG. 1. (a) Non-Abelian holonomy in a degenerate Hermitian system that possesses triple-degenerate energy sheets with real eigenvalues. The eigenfunctions at the starting and ending point (circle) are defined as  $|\psi_{i,1}\rangle$ ,  $|\psi_{i,2}\rangle$ , and  $|\psi_{i,3}\rangle$ , where the subscript “ $i$ ” indicates that they all occupy the  $i$ th energy level, while the number denotes the degenerate level. The lower panel shows the non-Abelian holonomy induced switching of eigenstates. (b) Non-Abelian holonomy in a nondegenerate non-Hermitian system with three nondegenerate energy sheets and two EPs. The holonomy induced switching of the three eigenstates  $|\psi_{i,1}\rangle$ ,  $|\psi_{j,1}\rangle$ , and  $|\psi_{k,1}\rangle$  is enabled by encircling the two EPs. (c) Non-Abelian holonomy in a degenerate non-Hermitian system having three triple-degenerate energy sheets that are connected by two DEPs, each of which is also triple-degenerate. By encircling the two DEPs, the holonomy results in the switching of eigenstates simultaneously between different energy levels and degenerate levels.

group  $D_4$ , which is revealed to be constructed by the interplay between two Abelian groups associated with the energy level and degenerate level, respectively. We have exploited femtosecond laser direct writing techniques to fabricate non-Hermitian photonic waveguides to demonstrate the features of the holonomy.

*Building block of a non-Abelian holonomic system*—We start by studying a three-state non-Hermitian system with a Hamiltonian

$$H_0 = \begin{bmatrix} \beta_0 + i\gamma & \kappa_{AB} & 0 \\ \kappa_{AB} & \beta_0 + \delta & \kappa_{BC} \\ 0 & \kappa_{BC} & \beta_0 + i\gamma \end{bmatrix}, \quad (1)$$

which can be realized using three single-mode paraxial photonic waveguides A, B, and C as illustrated in Fig. 2(a). Here, the waveguides A and C are assigned with position-dependent losses weighed by  $\gamma(z)$ , the waveguide B is introduced with a position-dependent detuning  $\delta(z)$ , and the coupling strengths

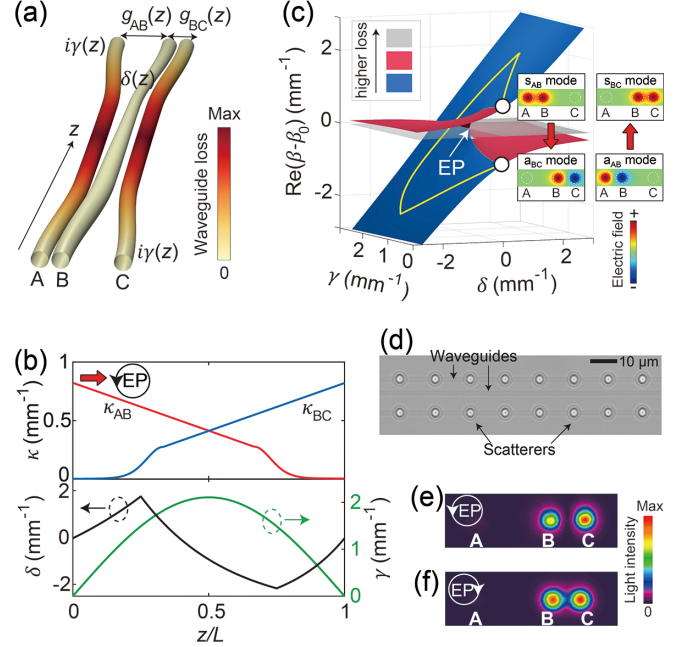


FIG. 2. (a) Schematic diagram of a non-Hermitian system consisting of three photonic waveguides. (b) The position-dependent coupling coefficients  $\kappa_{AB}$  and  $\kappa_{BC}$ , detuning  $\delta$  and non-Hermitian loss  $\gamma$  in the Hamiltonian of Eq. (1). The symbol  $L$  is the length of the system. (c) The calculated real part of the eigenvalues as a function of  $\delta$  and  $\gamma$ , with  $\sqrt{\kappa_{AB}^2 + \kappa_{BC}^2} = 0.78 \text{ mm}^{-1}$ . The eigenfield distributions indicate the mode switching behavior in (a) where an EP is encircled following the yellow path. (d) A local microscopic photograph of the fabricated samples. (e),(f) The measured output light diffraction patterns of the non-Hermitian system with  $L = 25 \text{ mm}$  when a  $s_{AB}$  mode (e) or an  $a_{AB}$  mode (f) is injected.

between adjacent waveguides are denoted by  $\kappa_{AB}(z)$  and  $\kappa_{BC}(z)$ . These parameters along the wave propagating direction (i.e.,  $+z$  axis) are presented in Fig. 2(b). The eigenvalues of the Hamiltonian, which are also the propagation constants of the coupled waveguides, are  $\beta_{1,2} = \beta_0 + \frac{1}{2}(\delta + i\gamma \pm \sqrt{4\kappa_{AB}^2 + 4\kappa_{BC}^2 + \delta^2 - \gamma^2 - 2i\delta\gamma})$  and  $\beta_3 = \beta_0 + i\gamma$ , where  $\beta_0$  is the eigenvalue of a nondetuned lossless waveguide ( $\approx 11.7 \text{ } \mu\text{m}^{-1}$ ). The system supports an EP at  $\delta = 0$  and  $\gamma = \sqrt{4\kappa_{AB}^2 + 4\kappa_{BC}^2}$ , and the choice of the parameter combinations in Fig. 2(b) is to encircle this EP in a  $\delta - \gamma$  parameter space for mode switching.

We assume the term  $\kappa_{AB}^2 + \kappa_{BC}^2$  to be a constant and plot the calculated real part of the eigenvalues as a function of  $\delta$  and  $\gamma$  in Fig. 2(c). The blue and gray energy sheets represent the eigenstate with lowest and highest losses, respectively. When we set a symmetric mode located in the waveguides A and B (namely  $s_{AB}$  mode, which is an eigenmode of the system) at the input port, its adiabatic evolution in the system follows the yellow path in Fig. 2(c) that encircles an EP in counterclockwise. The topology around the EP adiabatically switches the injected  $s_{AB}$  mode

to an output mode localized in the waveguides B and C with an antisymmetric phase distribution, namely  $a_{BC}$  mode. The counterpart process, i.e., adiabatic transformation from an  $a_{AB}$  mode to a  $s_{BC}$  mode, can be realized by reversing the sign of  $\delta$ , corresponding to the encirclement of the EP in clockwise [see the inset of Fig. 2(c)]. The above conclusion still holds when  $\kappa_{AB}^2 + \kappa_{BC}^2$  is not a constant (Supplemental Material [37], Fig. S1). We emphasize that all the holonomic processes in this Letter occur on the lowest-loss energy sheet and the evolution loop is far away from the EP. In this way, possible nonadiabatic transitions could be avoided (see Supplemental Material [37], Sec. I for discussions).

We fabricated the three photonic waveguides inside borosilicate glass by employing the femtosecond laser direct writing technique [18,19,38,39]. The coupling strength and detuning are respectively controlled by the gap distance and the moving speed of laser, while the non-Hermitian losses are introduced by writing position-dependent scatterers inside the waveguide [see Fig. 2(d),

also Supplemental Material [37], Sec. II, for experimental details]. We fabricated two samples featuring the encirclement of the EP in counterclockwise and clockwise, in which the  $s_{AB}$  mode and  $a_{AB}$  mode are excited, respectively. The measured light diffraction patterns at the output facet with working wavelength of 808 nm are shown in Figs. 2(e) and 2(f). Since these patterns do not contain the phase information, the symmetry of the mode is identified by examining the light intensity in the gap between two waveguides, i.e., a symmetric mode exhibits a field enhancement in the gap but the antisymmetric mode does not because of destructive interference. Based on this principle, the outputs in Figs. 2(e) and 2(f) are found to be antisymmetric mode and symmetric mode, respectively, in accordance with theoretical predictions.

*Design and experimental realization of non-Abelian holonomy in degenerate non-Hermitian systems*—The proposed three-state system can be used as a building block to construct a six-state non-Hermitian system with a Hamiltonian

$$H = \begin{bmatrix} \beta_0 + \delta_A + i\gamma_A & \kappa_{AB} & 0 & 0 & \kappa_{AX} & 0 \\ \kappa_{AB} & \beta_0 + \delta_B + i\gamma_B & 0 & 0 & 0 & \kappa_{BY} \\ 0 & 0 & \beta_0 + \delta_C + i\gamma_C & \kappa_{CD} & \kappa_{CX} & 0 \\ 0 & 0 & \kappa_{CD} & \beta_0 + \delta_D + i\gamma_D & 0 & \kappa_{DY} \\ \kappa_{AX} & 0 & \kappa_{CX} & 0 & \beta_0 + \delta_X + i\gamma_X & 0 \\ 0 & \kappa_{BY} & 0 & \kappa_{DY} & 0 & \beta_0 + \delta_Y + i\gamma_Y \end{bmatrix}. \quad (2)$$

The cross section and Hamiltonian parameters are shown in Figs. 3(a) and 3(b), respectively. At the starting and ending point of the holonomy, the system supports degenerate symmetric modes  $s_{AB}$  and  $s_{CD}$ , and degenerate antisymmetric modes  $a_{AB}$  and  $a_{CD}$ . The consequence of non-Abelian holonomy in degenerate non-Hermitian systems is the switching of eigenstates simultaneously between different energy levels (e.g., “s” or “a” here) and degenerate levels (e.g., mode location in “AB” or “CD” here), therefore the outcome is a mode transformation between  $s_{AB}$  and  $a_{CD}$ , and that between  $s_{CD}$  and  $a_{AB}$ . The whole holonomic process can be divided into three steps. In each step, there are two uncoupled three-state building blocks that implement the pumping of eigenmodes while guaranteeing double-degenerate energy levels. At step I, the waveguides A, B, and X form a building block in which an injected  $s_{AB}$  (or  $a_{AB}$ ) mode is transformed to an  $a_{AX}$  (or  $s_{AX}$ ) mode, while the left three waveguides form another building block, leading to a conversion from the  $s_{CD}$  (or  $a_{CD}$ ) mode to the  $a_{DY}$  (or  $s_{DY}$ ) mode. Step II enables a transformation of the eigenmodes from waveguides “AX” (or “DY”) to “CX” (or “BY”), while in step III the eigenmodes located in waveguides “CX” (or “BY”) are pumped to “CD” (or

“AB”). After the three steps, the location of the eigenmode is exchanged between that in waveguides “AB” and “CD,” together with a change in the mode symmetry. In this way, a non-Abelian holonomic process with two energy levels and two degenerate levels is accomplished.

Figure 3(c) shows the calculated eigenvalues of the Hamiltonian in the holonomic process, where each energy band is double-degenerate. Following the blue band, the  $s_{AB}$  (or  $s_{CD}$ ) mode is adiabatically transformed to the  $a_{CD}$  (or  $a_{AB}$ ) mode (see Fig. S11 in Supplemental Material [37] for more details), while the opposite process, from the  $a_{AB}$  (or  $a_{CD}$ ) mode to the  $s_{CD}$  (or  $s_{AB}$ ) mode, occurs along the red band. This holonomy with two energy levels and two degenerate levels is illustrated in Fig. 3(d), and is also numerically simulated in Fig. 3(e) (see Supplemental Material [37], Sec. II, for simulation details). The attenuation in the light intensity induced by the non-Hermitian losses could be alleviated by using a Hamiltonian hopping method [34].

We fabricated the above system with its schematic and microscope photographs presented in Fig. 4(a). To demonstrate details of the holonomy, three samples are fabricated with lengths of 25 mm, 50 mm, and 75 mm, respectively: the

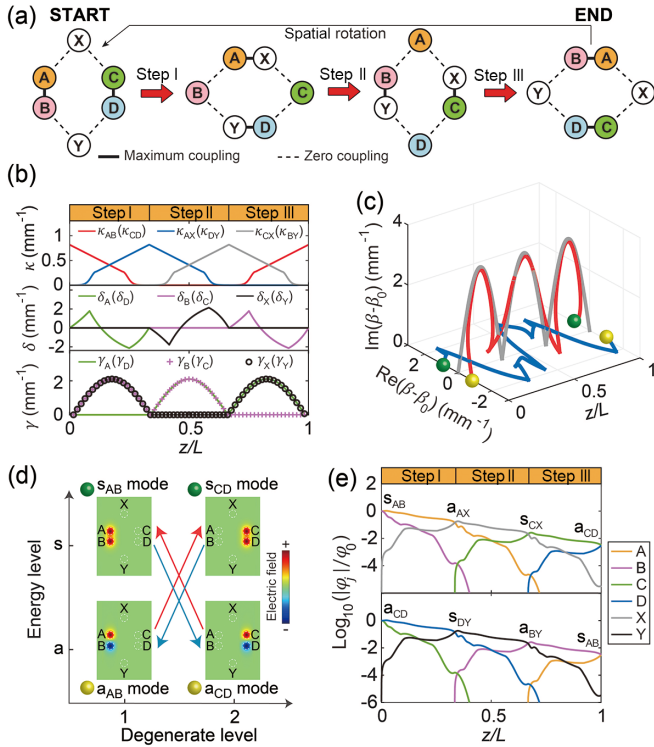


FIG. 3. (a) Cross section of the designed non-Abelian holonomic system. (b) The Hamiltonian parameters along the waveguiding direction. (c) Calculated eigenvalues of the non-Hermitian Hamiltonian in Eq. (2). (d) The proposed non-Abelian holonomy with two energy levels and two degenerate levels. The inset shows the eigenfield distributions of the four eigenmodes and the arrow marks the holonomy induced mode switching direction, where the arrow color coincides with that in (c). (e) The calculated state vector  $|\varphi(z)\rangle = [\varphi_A, \varphi_B, \varphi_C, \varphi_D, \varphi_X, \varphi_Y]^T$  in the holonomic process with the  $s_{AB}$  mode (upper panel) and  $s_{CD}$  mode (lower panel) as the input, where  $\varphi_0$  denotes the amplitude of the input.

first sample contains step I only, the second one contains steps I and II, and the third sample contains all three steps. In this way, measuring the light diffraction patterns at the output facet of each step is available. The measured results with injected  $s_{AB}$  and  $s_{CD}$  modes are shown in Figs. 4(b) and 4(c), respectively, which clearly demonstrate their evolutions to the final  $a_{CD}$  and  $a_{AB}$  modes. We also fabricated another system with reversed detuning while other Hamiltonian parameters are kept the same, to demonstrate the process from an input  $a_{AB}$  ( $a_{CD}$ ) mode to an output  $s_{CD}$  ( $s_{AB}$ ) mode [Figs. 4(d) and 4(e)]. These two systems with opposite detuning parameters share the same holonomy induced mode switching behavior (Supplemental Material [37], Sec. I). Therefore, we have combined them to demonstrate the full holonomy in experiments.

*Non-Abelian group and its non-Abelian features*—By choosing different Hamiltonian parameters, the proposed six-state non-Hermitian system can realize eight holonomic processes that form a non-Abelian group  $D_4 = \{E, R_1, R_2, R_3, H, V, D, D'\}$ , as depicted in Fig. 5(a).

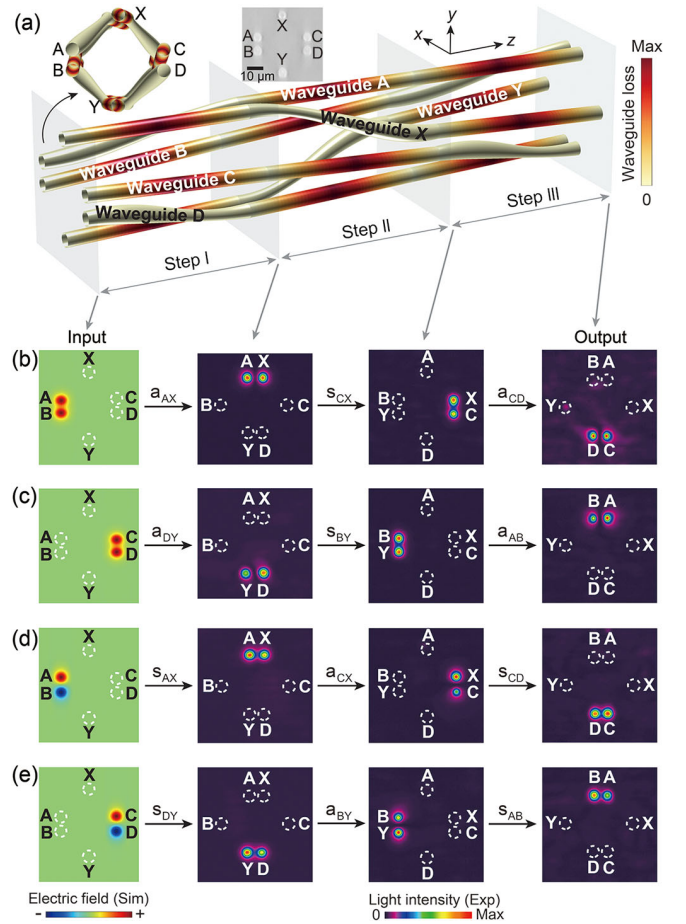


FIG. 4. (a) Schematic diagram of the non-Hermitian system designed following the Hamiltonian of Eq. (2). (b)–(e) Experimentally measured light output patterns at the end of steps I, II, and III (from left to right) when the input is the  $s_{AB}$  mode (b),  $s_{CD}$  mode (c),  $a_{AB}$  mode (d), and  $a_{CD}$  mode (e).

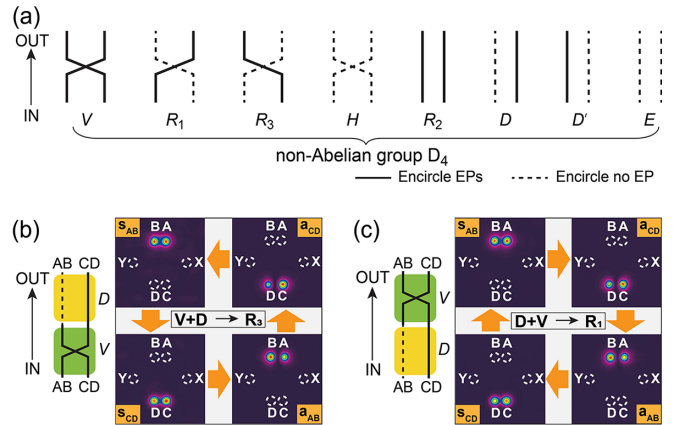


FIG. 5. (a) Schematic diagram of all the eight holonomic processes available using the proposed system, forming a non-Abelian group  $D_4$ . (b) Experimentally measured light output patterns in a system consisting of the  $V$  operation and  $D$  operation successively, where each arrow marks a process from an input to a measured outcome. (c) Same as (b) except that the sequence of the two operations is swapped.

The aforementioned holonomic process is represented by the group element  $V$ , where the crossing of two lines indicates the switching between the eigenmodes in waveguides “AB” and “CD,” while the solid line denotes that an EP is encircled. Besides, we use two parallel lines to depict the case that the eigenmodes located in waveguides “AB” and “CD” are not switched, and the case in which no EP is encircled is denoted by a dashed line.

We show how this non-Abelian group can be constructed by two Abelian groups that are respectively associated with the 2 degrees of freedom of the holonomy, i.e., the degenerate level and the energy level. We define the eigenfunction of a symmetric mode and an antisymmetric

mode as  $|\psi_s\rangle = [1, 0]^T$  and  $|\psi_a\rangle = [0, 1]^T$ , respectively. Meanwhile, the eigenfunction of the mode localized in waveguides “AB” and “CD” is defined as  $|\psi_{AB}\rangle = [1, 0]^T$  and  $|\psi_{CD}\rangle = [0, 1]^T$ , respectively. Using these bases, the four working eigenmodes at the start and end point of the holonomy can be generated via  $|\psi_{s,AB}\rangle = |\psi_s\rangle \otimes |\psi_{AB}\rangle$ ,  $|\psi_{s,CD}\rangle = |\psi_s\rangle \otimes |\psi_{CD}\rangle$ ,  $|\psi_{a,AB}\rangle = |\psi_a\rangle \otimes |\psi_{AB}\rangle$ , and  $|\psi_{a,CD}\rangle = |\psi_a\rangle \otimes |\psi_{CD}\rangle$  (e.g.,  $|\psi_{s,AB}\rangle$  represents the eigenfunction of the  $s_{AB}$  mode). The transformation matrix connecting the outcome and input of the holonomy is written as (see Supplemental Material [37], Sec. III, for derivation details)

$$U_{i,j,k} = U_{EP}U_{DEG} = \left( M_i^{EP} \otimes \begin{bmatrix} 1 & 0 \\ 0 & 0 \end{bmatrix} + M_j^{EP} \otimes \begin{bmatrix} 0 & 0 \\ 0 & 1 \end{bmatrix} \right) \left( \begin{bmatrix} 1 & 0 \\ 0 & 1 \end{bmatrix} \otimes M_k^{DEG} \right), \quad \{i, j, k = 0, 1\}, \quad (3)$$

where  $U_{EP}$  and  $U_{DEG}$  are generating matrix from the EP associated energy level and degenerate level, respectively. In Eq. (3), we have introduced EP associated operators  $M_1^{EP} = \begin{bmatrix} 0 & 1 \\ 1 & 0 \end{bmatrix}$  and  $M_0^{EP} = \begin{bmatrix} 1 & 0 \\ 0 & 1 \end{bmatrix}$ , which deal with case that an EP is encircled or not, respectively (e.g.,  $M_1^{EP}|\psi_s\rangle = |\psi_a\rangle$ ). Degenerate level associated operators  $M_1^{DEG} = \begin{bmatrix} 0 & 1 \\ 1 & 0 \end{bmatrix}$  and  $M_0^{DEG} = \begin{bmatrix} 1 & 0 \\ 0 & 1 \end{bmatrix}$  are also used to deal with the case that a location change is induced or not (e.g.,  $M_1^{DEG}|\psi_{AB}\rangle = |\psi_{CD}\rangle$ ).

Equation (3) gives rise to all the eight group elements in Fig. 5(a). For instance, the element  $V$  is constructed by setting  $i = 1$ ,  $j = 1$ , and  $k = 1$ , which satisfies  $|\psi_{a,CD}\rangle = U|\psi_{s,AB}\rangle$ . The generated matrix from Eq. (3) is also the holonomy induced Berry-Wilczek-Zee geometric phase matrix, i.e., a unitary matrix connecting the input and output of the holonomy (Supplemental Material [37], Sec. IV). The geometric phase matrix associated with each group element is summarized in Table S1 and discussed in Supplemental Material [37], Sec. V, while the multiplication table of the non-Abelian group is given in Table S2.

The non-Abelian feature of the group can be demonstrated experimentally by cascading two or more different holonomic processes. Without loss of generality, we combine the group element  $V$  and  $D$ . Figure 5(b) shows the experimental results in a cascaded sample where the  $V$  operation and  $D$  operation are executed successively. When we inject the  $s_{AB}$ ,  $s_{CD}$ ,  $a_{AB}$ , and  $a_{CD}$  mode, the output is found to be the  $s_{CD}$ ,  $a_{AB}$ ,  $a_{CD}$ , and  $s_{AB}$  mode, respectively. Since the two group elements are noncommutative, swapping their order will result in distinct outcomes. The corresponding experimental results are given in Fig. 5(c), where the symmetry of all the output modes is different from those in Fig. 5(b). The non-Abelian feature can also be revealed by cascading any other two or more group elements that are noncommutative.

*Conclusion*—To conclude, we have proposed the design and experimental realization of a non-Abelian holonomy with two energy levels and two degenerate levels. The holonomy induced mode switching between eigenmodes belonging to different DEPs has been experimentally observed. The non-Abelian feature has been demonstrated by cascading two noncommutative systems. The energy levels and degenerate levels in the holonomy can be further increased by introducing more DEPs or higher-order DEPs and thus discrete non-Abelian groups with more elements could be achieved. The multiple energy levels, i.e., the new degree of freedom in non-Abelian holonomy, are expected to inspire new non-Abelian applications (Supplemental Material [37], Sec. VI).

*Acknowledgments*—This work was supported by the Young Top-Notch Talent for Ten Thousand Talent Program (X. L. Z. and Z. N. T.), National Natural Science Foundation of China (Grants No. 12374350, No. 61827826, No. 62131018, No. 623B2042) and the Major Science and Technology Projects in Jilin Province (20220301002GX).

- [1] Y. Aharonov and D. Bohm, *Phys. Rev.* **115**, 485 (1959).
- [2] F. Wilczek and A. Zee, *Phys. Rev. Lett.* **52**, 2111 (1984).
- [3] Y. Aharonov and J. Anandan, *Phys. Rev. Lett.* **58**, 1593 (1987).
- [4] L. O’Raifeartaigh and N. Straumann, *Rev. Mod. Phys.* **72**, 1 (2000).
- [5] M. V. Berry, *Proc. R. Soc. London* **392**, 45 (1984).
- [6] C. N. Yang and R. L. Mills, *Phys. Rev.* **96**, 191 (1954).
- [7] H. Georgi, *Phys. Today* **41**, No. 4, 29 (1988).
- [8] J. Pachos, P. Zanardi, and M. Rasetti, *Phys. Rev. A* **61**, 010305(R) (1999).
- [9] P. Zanardi and M. Rasetti, *Phys. Lett. A* **264**, 94 (1999).

- [10] Y.-J. Lin, R. L. Compton, K. Jiménez-García, J. V. Porto, and I. B. Spielman, *Nature (London)* **462**, 628 (2009).
- [11] J. Dalibard, F. Gerbier, G. Juzeliūnas, and P. Öhberg, *Rev. Mod. Phys.* **83**, 1523 (2011).
- [12] Z.-G. Chen, R.-Y. Zhang, C. T. Chan, and G. Ma, *Nat. Phys.* **18**, 179 (2022).
- [13] O. You, S. Liang, B. Xie, W. Gao, W. Ye, J. Zhu, and S. Zhang, *Phys. Rev. Lett.* **128**, 244302 (2022).
- [14] A. A. Abdumalikov Jr, J. M. Fink, K. Juliusson, M. Pechal, S. Berger, A. Wallraff, and S. Filipp, *Nature (London)* **496**, 482 (2013).
- [15] Y. Yang, C. Peng, D. Zhu, H. Buljan, J. D. Joannopoulos, B. Zhen, and M. Soljačić, *Science* **365**, 1021 (2019).
- [16] M. Kremer, L. Teuber, A. Szameit, and S. Scheel, *Phys. Rev. Res.* **1**, 033117 (2019).
- [17] V. Brosco, L. Pilozzi, R. Fazio, and C. Conti, *Phys. Rev. A* **103**, 063518 (2021).
- [18] X.-L. Zhang, F. Yu, Z.-G. Chen, Z.-N. Tian, Q.-D. Chen, H.-B. Sun, and G. Ma, *Nat. Photonics* **16**, 390 (2022).
- [19] Y.-K. Sun, X.-L. Zhang, F. Yu, Z.-N. Tian, Q.-D. Chen, and H.-B. Sun, *Nat. Phys.* **18**, 1080 (2022).
- [20] V. Neef, J. Pinske, F. Klauck, L. Teuber, M. Kremer, M. Ehrhardt, M. Heinrich, S. Scheel, and A. Szameit, *Nat. Phys.* **19**, 30 (2023).
- [21] C. M. Bender and S. Boettcher, *Phys. Rev. Lett.* **80**, 5243 (1998).
- [22] M. V. Berry, *Czech. J. Phys.* **54**, 1039 (2004).
- [23] I. I. Arkhipov, A. Miranowicz, F. Minganti, S. K. Ozdemir, and F. Nori, *Nat. Commun.* **14**, 2076 (2023).
- [24] C. Dembowski, H.-D. Gräf, H. L. Harney, A. Heine, W. D. Heiss, H. Rehfeld, and A. Richter, *Phys. Rev. Lett.* **86**, 787 (2001).
- [25] T. Gao, E. Estrecho, K. Y. Bliokh, T. C. H. Liew, M. D. Fraser, S. Brodbeck, M. Kamp, C. Schneider, S. Höfling, Y. Yamamoto, F. Nori, Y. S. Kivshar, A. G. Truscott, R. G. Dall, and E. A. Ostrovskaya, *Nature (London)* **526**, 554 (2015).
- [26] K. Ding, G. Ma, M. Xiao, Z. Q. Zhang, and C. T. Chan, *Phys. Rev. X* **6**, 021007 (2016).
- [27] W. Tang, X. Jiang, K. Ding, Y.-X. Xiao, Z.-Q. Zhang, C. T. Chan, and G. Ma, *Science* **370**, 1077 (2020).
- [28] K. Ding, C. Fang, and G. Ma, *Nat. Rev. Phys.* **4**, 745 (2022).
- [29] J. Doppler, A. A. Mailybaev, J. Böhm, U. Kuhl, A. Girschik, F. Libisch, T. J. Milburn, P. Rabl, N. Moiseyev, and S. Rotter, *Nature (London)* **537**, 76 (2016).
- [30] X.-L. Zhang, S. Wang, B. Hou, and C. T. Chan, *Phys. Rev. X* **8**, 021066 (2018).
- [31] J. W. Yoon, Y. Choi, C. Hahn, G. Kim, S. H. Song, K.-Y. Yang, J. Y. Lee, Y. Kim, C. S. Lee, J. K. Shin, H.-S. Lee, and P. Berini, *Nature (London)* **562**, 86 (2018).
- [32] H. Nasari, G. Lopez-Galmiche, H. E. Lopez-Aviles, A. Schumer, A. U. Hassan, Q. Zhong, S. Rotter, P. LiKamWa, D. N. Christodoulides, and M. Khajavikhan, *Nature (London)* **605**, 256 (2022).
- [33] F. Yu, X.-L. Zhang, Z.-N. Tian, Q.-D. Chen, and H.-B. Sun, *Phys. Rev. Lett.* **127**, 253901 (2021).
- [34] A. Li, J. Dong, J. Wang, Z. Cheng, J. S. Ho, D. Zhang, J. Wen, X. L. Zhang, C. T. Chan, A. Alù, C. W. Qiu, and L. Chen, *Phys. Rev. Lett.* **125**, 187403 (2020).
- [35] R. Uzdin, A. Mailybaev, and N. Moiseyev, *J. Phys. A* **44**, 435302 (2011).
- [36] W. Tang, K. Ding, and G. Ma, *Natl. Sci. Rev.* **9**, nwc010 (2022).
- [37] See Supplemental Material at <http://link.aps.org/supplemental/10.1103/PhysRevLett.133.053802> for details, including Sec. I, nonadiabatic transitions in the holonomic process; Sec. II, experimental and simulation details; Sec. III, generation of the non-Abelian group  $D_4$ ; Sec. IV, non-Hermitian Berry-Wilczek-Zee (BWZ) phase matrix; Sec. V, details of the non-Abelian group  $D_4$ ; Sec. VI, proposal of non-Hermitian non-Abelian braiding; Sec. VII, double degeneracy of the non-Hermitian Hamiltonian; Sec. VIII, supplemental tables; and Sec. IX, supplemental figures.
- [38] K. M. Davis, K. Miura, N. Sugimoto, and K. Hirao, *Opt. Lett.* **21**, 1729 (1996).
- [39] M. C. Rechtsman, J. M. Zeuner, Y. Plotnik, Y. Lumer, D. Podolsky, F. Dreisow, S. Nolte, M. Segev, and A. Szameit, *Nature (London)* **496**, 196 (2013).